Commutation errors in Large Eddy Simulation on moving grids : Application to piston engine flows

By V. R. Moureau †, O. V. Vasilyev ‡ C. Angelberger ¶ AND T. J. Poinsot ‖

A theoretical framework is developed to evaluate the Temporal Commutation Errors (TCE) in piston-engine flows. These errors occur when the Large-Eddy Simulation (LES) filter is a function of time, implying for the temporal partial derivative not to commute with filtering. TCE are derived for structured and unstructured grids, highlighting the contributions of width and shape variations. Finally they are evaluated on LES simulations of a square-piston experiment and the influence of the crank speed and the compression ratio are studied. It is found that the TCE may be neglected to first order if the flow field and mesh deformation are generated by the same boundary movement.

1. Introduction

The design of modern combustion devices with the aim to reduce fuel consumption and pollutant emissions is often complicated by combustion instabilities and more generally by the intrinsic unsteadiness. This is the case of industrial or aeronautic gas turbines, rocket engines and piston engines. Large-Eddy Simulation (LES) may become a key tool that could give engineers the means to better predict operation ranges and specifications. Recent improvements of LES codes have shown encouraging simulations of gas turbines (Kaufmann *et al.* 2002; Selle *et al.* 2004; Prière *et al.* 2004) but in spite of these first successes further developments are needed before obtaining satisfactory results, *e.g.* on realistic piston-engine geometries (Celik *et al.* 2001). This gap can be explained by the fact that piston-engine flows are very confined and walls play therefore a major role. Moreover piston-engine combustion chambers are strongly deformed while operating and that induces big pressure variations and meshing problems.

The LES principle is to reduce the simulation time compared to Direct Numerical Simulations (DNS) by filtering the governing equations, resulting in a reduction of the spectral content of the flow. Then the difficulty is to model the effects of the removed small scales on the resolved large eddies. Supposing that the filtering operator commutes with partial derivatives, the filtered equations are similar to unfiltered ones with unclosed extra terms. The Smagorinsky model (Smagorinsky 1963) is commonly used for turbulent unclosed terms in the momentum equation. The assumption that filtering commutes with partial derivatives is generally considered valid on fixed grids with uniform cell width. On deforming unstructured grids this is not the case anymore and commutation errors may have to be considered. In the past spatial commutation errors (SCE) have extensively been studied with the aim to apply LES to complex geometries. The first theoretical analysis is due to Ghosal (Ghosal & Moin 1995; Ghosal 1999) who has given the order of convergence of SCE on structured grids. Some numerical estimations of SCE can also

† IFP and CERFACS, 42 av. G. Coriolis, 31057 Toulouse CEDEX
‡ University of Colorado at Boulder, UCB 427, Boulder, CO 80309
¶ IFP, 1 et 4 av. Bois Preau, 92500 Rueil Malmaison
‖ IMF Toulouse, INP de Toulouse and CNRS, 31400 Toulouse CEDEX, France

be found for turbulent channel flows (Fureby & Tabor 1997). Then the SCE derivation formalism has been improved to deal with boundaries, and commutating filters have been defined for structured grids (Vasilyev *et al.* 1998) and unstructured grids (Marsden *et al.* 2002; Haselbacher & Vasilyev 2003). The most recent developments have been focused on the local spectrum of SCE (Vasilyev & Goldstein 2004) and the influence of filter shape or width variations on spectral content has been highlighted.

Because most LES computations have been performed on fixed meshes, very few studies on temporal commutation errors (TCE) are available. Their possible importance in piston-engine simulations has been stressed by Franke (Franke & Frank 2001) but no evaluation on realistic geometry has been carried out. TCE are a priori increasing with the instantaneous deformation rate of the mesh as SCE are increasing with filter-width spatial stretching. This deformation rate is itself a function of crank speed and compression ratio.

This study aims at quantifying TCE in a piston-engine like geometry. First TCE are derived for different grid types ordered by increasing connectivity complexity : one dimensional grids (Section 2), three-dimensional structured grids (Section 3) and three-dimensional unstructured grids (Section 4). Then TCE for the momentum equation are evaluated on a piston-engine like configuration (Section 5), consisting of a square-piston engine for which experimental data are available. Since the DNS of this type of experiment is not feasible, the exact derivation of TCE could not be computed directly. Instead an *a priori* model for TCE is proposed and evaluated in LES simulations of the square-piston experiment for different crank speeds and compression ratios.

2. One dimensional derivation

As a first step TCE are studied for one dimensional grids. Given a function ϕ of space and time the filtered function $\overline{\phi}$ is defined by the following convolution product :

$$\overline{\phi}(x,t) = \frac{1}{\Delta(x,t)} \int_{a(t)}^{b(t)} G\left(\frac{x-y}{\Delta(x,t)}, x, t\right) \phi(y,t) dy \tag{2.1}$$

The filter G is assumed to have the most general form, *i.e.* non-uniform filter width and shape. In Eq. (2.1) the variable filter width Δ has been taken out of the filter, which thus only contains information about its shape. This is justified by the fact that width and shape variations do not have the same influence on the local spectrum (Vasilyev & Goldstein 2004) and that the shape is often supposed constant during simulations. Then TCE are defined by :

$$\mathrm{TCE}[\phi] = \overline{\frac{\partial \phi}{\partial t}} - \frac{\partial \overline{\phi}}{\partial t} \tag{2.2}$$

To obtain an expression for TCE it is necessary to change the non-uniform space $[a(t), b(t)]$ into a uniform mapping space $[A(x,t), B(x,t)]$ with the change of variables :

$$\xi = \frac{x-y}{\Delta(x,t)}, \quad A(x,t) = \frac{x-a(t)}{\Delta(x,t)}, \quad B(x,t) = \frac{x-b(t)}{\Delta(x,t)} \tag{2.3}$$

Then the filtering process can be rewritten :

$$\overline{\phi}(x,t) = \int_{A(x,t)}^{B(x,t)} G(\xi, x, t)\, \phi(x - \Delta(x,t)\xi, t) d\xi \tag{2.4}$$

And if $\phi(x-\Delta(x,t)\xi,t)$ can be expanded in Taylor series :

$$\phi(x-\Delta(x,t)\xi,t)=\sum_{k=0}^{\infty}\frac{(-1)^k\Delta^k(x,t)\xi^k}{k!}\frac{\partial^k\phi}{\partial x^k}(x,t) \tag{2.5}$$

Introducing the filter moments $\mathcal{M}^{(k)}$:

$$\mathcal{M}^{(k)}(x,t)=-\int_{A(x,t)}^{B(x,t)}G\left(\xi,x,t\right)\xi^k d\xi \tag{2.6}$$

$\overline{\phi}$ can be expressed as a series expansion of spatial partial derivatives of ϕ :

$$\overline{\phi}(x,t)=-\sum_{k=0}^{\infty}\frac{(-1)^k\Delta^k(x,t)}{k!}\mathcal{M}^{(k)}(x,t)\frac{\partial^k\phi}{\partial x^k}(x,t) \tag{2.7}$$

The series' convergence in Eq. (2.5) and Eq. (2.7) has been discussed by Vasilyev (Vasilyev *et al.* 1998). Using the fact that turbulent flows have a bounded spectrum, the authors have demonstrated that the convergence of Eq. (2.5) is absolute and thus uniform even if Δ is spatially varying. They have also proven that Eq. (2.7) converges for arbitrary Δ if the filter has a finite support. If the filter has an infinite support but the filter moments do not grow faster than factorial (*e.g.* the Gaussian filter) then the series converges provided that Δ is less than a number of Kolmogorov scales. Finally if ϕ is spectrally bounded then $\partial\phi/\partial t$ is also spectrally bounded and Eq. (2.7) can therefore be used to reformulate TCE :

$$\mathrm{TCE}[\phi]=-\sum_{k=0}^{\infty}\frac{(-1)^k}{k!}\left[\Delta^k(x,t)\mathcal{M}^{(k)}(x,t)\frac{\partial^k}{\partial x^k}\frac{\partial\phi}{\partial t}-\frac{\partial}{\partial t}\left(\Delta^k(x,t)\mathcal{M}^{(k)}(x,t)\frac{\partial^k\phi}{\partial x^k}\right)\right] \tag{2.8}$$

$$\mathrm{TCE}[\phi]=\sum_{k=1}^{\infty}\frac{(-1)^k}{k!}\frac{\partial}{\partial t}\left(\Delta^k(x,t)\mathcal{M}^{(k)}(x,t)\right)\frac{\partial^k\phi}{\partial x^k} \tag{2.9}$$

In Eq. (2.9) the filter width $\Delta(x,t)$ is a function of time and of the Eulerian abscissa x. But $\Delta(x,t)$ is generally a function of the local cell volume and on deforming grids the cells are moving and stretching. It is therefore more convenient to introduce the Arbitrary Lagrangian-Eulerian (ALE) coordinate $X(x,t)$ to express the filter width $\Delta(x,t)=\delta(X,t)$. If $\delta(X,t)$ is equal to the cell volume $V_\omega(X,t)$ multiplied by a constant factor then $\delta(X,t)$ can be written as a function of cell-volume spatial variations and of the mean deformation rate $\overline{\nabla\cdot\dot{X}}$:

$$\frac{\partial\Delta}{\partial t}(x,t)=\frac{\partial\,\delta\left(X(x,t),t\right)}{\partial t}=\dot{X}\frac{\partial\delta}{\partial X}+\delta(X,t)\overline{\nabla\cdot\dot{X}} \tag{2.10}$$

where the mean deformation rate is defined by :

$$\overline{\nabla\cdot\dot{X}}=\frac{1}{\delta(X,t)}\frac{\partial\delta}{\partial t}(X,t)=\frac{1}{\omega(X,t)}\int_{\omega(X,t)}\frac{\partial\dot{X}}{\partial x}dx \tag{2.11}$$

In Eq. (2.10) the first right-hand term is due to the cell translation and the spatial stretching and the second is due to the cell contraction or dilatation. Then TCE can be

decomposed into three different contributions :

$$\begin{aligned}\mathrm{TCE}[\phi] = (\overline{\nabla \cdot \dot{X}}) \sum_{k=1}^{\infty} \frac{(-1)^k \delta^k}{(k-1)!}\, \mathcal{M}^{(k)}(x,t) \frac{\partial^k \phi}{\partial x^k} \\ + \dot{X} \sum_{k=1}^{\infty} \frac{(-1)^k \delta^{(k-1)}}{(k-1)!}\, \frac{\partial \delta}{\partial X} \mathcal{M}^{(k)}(x,t) \frac{\partial^k \phi}{\partial x^k} \\ + \sum_{k=1}^{\infty} \frac{(-1)^k \delta^k}{k!}\, \frac{\partial \mathcal{M}^{(k)}}{\partial t}(x,t) \frac{\partial^k \phi}{\partial x^k}\end{aligned} \tag{2.12}$$

The first right-hand term arises from the cell temporal stretching. Its sign depends on the deformation type : contraction or dilatation. The second term is a spatial commutation error multiplied by the translation speed of the cell. This term is zero on uniform grids and when the mesh is not uniform it can be treated using a spatially commutative filter (Vasilyev *et al.* 1998; Marsden *et al.* 2002; Haselbacher & Vasilyev 2003). Finally the third term is due to shape variations. For example if during a simulation the filter shape changes from top-hat to Gaussian it will produce TCE through this third term. For simplicity the filter shape is assumed constant throughout the computations. The term of interest is therefore the first one which directly depends on the deformation rate of the combustion chamber.

3. Three dimensional derivation for structured grids

The TCE analysis of Section 2 can be performed in a very similar manner for multi dimensional structured grids because a filter width in each main direction can be easily defined. Then the differences come from the Taylor series expansion or from the filtering definition that becomes :

$$\overline{\phi}(\mathbf{x},t) = \frac{1}{\Delta_1(\mathbf{x},t)\Delta_2(\mathbf{x},t)\Delta_3(\mathbf{x},t)} \iiint_{\Omega_{\mathbf{x}}(t)} G\left(\frac{x_i - y_i}{\Delta_i(\mathbf{x},t)}, \mathbf{x}, t\right) \phi(\mathbf{y},t) d^3\mathbf{y} \tag{3.1}$$

where $\mathbf{x} = (x_1, x_2, x_3)^T$. Then the same change of variable $\Delta\boldsymbol{\xi} = (\Delta_i \xi_i)^T = (x_i - y_i)^T$ as for the one dimensional derivation can be carried out :

$$\overline{\phi}(\mathbf{x},t) = -\iiint_{\Omega_{\boldsymbol{\xi}}(\mathbf{x},t)} G(\boldsymbol{\xi},\mathbf{x},t)\, \phi(\mathbf{x} - \Delta\boldsymbol{\xi}, t)\, d^3\boldsymbol{\xi} \tag{3.2}$$

Using the gradient operator $\boldsymbol{\nabla}$, the Taylor expansion of $\phi(\mathbf{x} - \Delta\boldsymbol{\xi}, t)$ reads :

$$\begin{aligned}\phi(\mathbf{x} - \Delta\boldsymbol{\xi}, t) &= \sum_{l=0}^{\infty} \frac{(-1)^l}{l!} (\Delta\boldsymbol{\xi} \cdot \boldsymbol{\nabla})^l\, \phi(\mathbf{x},t) \\ &= \sum_{i=0}^{\infty}\sum_{j=0}^{\infty}\sum_{k=0}^{\infty} \frac{(-1)^{i+j+k}}{i!\, j!\, k!}\, (\Delta_1\xi_1)^i (\Delta_2\xi_2)^j (\Delta_3\xi_3)^k\, \nabla_1^i \nabla_2^j \nabla_3^k\, \phi(\mathbf{x},t)\end{aligned} \tag{3.3}$$

The 3D filter moments are defined as follows :

$$\mathcal{M}^{(ijk)}(\mathbf{x},t) = \iiint_{\Omega_{\boldsymbol{\xi}}(\mathbf{x},t)} G(\boldsymbol{\xi},\mathbf{x},t)\, \xi_1^i\, \xi_2^j\, \xi_3^k\, d^3\boldsymbol{\xi} \tag{3.4}$$

Finally the 3D equivalent of Eq. (2.9) which gives the Taylor expansion of TCE is

written :

$$\mathrm{TCE}[\phi] = \sum_{i=0}^{\infty}\sum_{j=0}^{\infty}\sum_{k=0}^{\infty} \frac{(-1)^{i+j+k}}{i!\,j!\,k!}\ \frac{\partial}{\partial t}\left[\Delta_1^i\Delta_2^j\Delta_3^k\mathcal{M}^{(ijk)}\right]\nabla_1^i\nabla_2^j\nabla_3^k\ \phi(\mathbf{x},t) \tag{3.5}$$

If the commutation errors that come from grid non-uniformity and filter shape variations are neglected then TCE can be reformulated as follows to have the mean deformation rate in each direction appear :

$$\mathrm{TCE}[\phi] = \sum_{i=0}^{\infty}\sum_{j=0}^{\infty}\sum_{k=0}^{\infty} \frac{(-1)^{i+j+k}}{i!\,j!\,k!}\ \left(i(\overline{\nabla\cdot\dot{X}})_1 + j(\overline{\nabla\cdot\dot{X}})_2 + k(\overline{\nabla\cdot\dot{X}})_3\right)$$
$$\delta_1^i\delta_2^j\delta_3^k\ \mathcal{M}^{(ijk)}\nabla_1^i\nabla_2^j\nabla_3^k\ \phi(\mathbf{x},t) \tag{3.6}$$

and the mean deformation rate of the cell ω in the direction i is :

$$(\overline{\nabla\cdot\dot{X}})_i = \frac{1}{\omega_i(\mathbf{X},t)}\int_{\omega_i(\mathbf{X},t)}\frac{\partial\dot{X}_i}{\partial x_i}\,dx_i \tag{3.7}$$

For symmetric filters ($\mathcal{M}^{(ijk)} = 0$ if i,j or k is odd) the TCE leading terms $\mathcal{L}$ of Eq. (3.6) are diffusive or anti-diffusive depending on the cell deformation :

$$\begin{aligned}\mathcal{L} = &(\overline{\nabla\cdot\dot{X}})_1\ \delta_1^2\ \mathcal{M}^{(2,0,0)}\ \nabla_1^2\phi(\mathbf{x},t)\\ &+(\overline{\nabla\cdot\dot{X}})_2\ \delta_2^2\ \mathcal{M}^{(0,2,0)}\ \nabla_2^2\phi(\mathbf{x},t)\\ &+(\overline{\nabla\cdot\dot{X}})_3\ \delta_3^2\ \mathcal{M}^{(0,0,2)}\ \nabla_3^2\phi(\mathbf{x},t)\end{aligned} \tag{3.8}$$

4. Three dimensional derivation for unstructured grids

The derivation of TCE for unstructured grids is different compared to structured grids because generally no main direction exists anymore. Only a unique filter width can be defined and it becomes useless to take this width out of the filter definition G. The filter width is therefore defined implicitely and the filtering convolution reads :

$$\overline{\phi}(\mathbf{x},t) = \iiint_{\Omega_{\mathbf{x}}(t)} G\left(\mathbf{x}-\mathbf{y},\mathbf{x},t\right)\phi(\mathbf{y},t)d^3\mathbf{y} \tag{4.1}$$

Then the filter width does not appear anymore in the variable change $\boldsymbol{\xi} = \mathbf{x}-\mathbf{y}$ to switch to the mapping space :

$$\overline{\phi}(\mathbf{x},t) = \iiint_{\Omega_{\boldsymbol{\xi}}(\mathbf{x},t)} G\left(\boldsymbol{\xi},\mathbf{x},t\right)\phi(\mathbf{x}-\boldsymbol{\xi},t)d^3\boldsymbol{\xi} \tag{4.2}$$

This is also the case in the Taylor expansion of $\phi(\mathbf{x}-\boldsymbol{\xi},t)$ that reads :

$$\phi(\mathbf{x}-\boldsymbol{\xi},t) = \sum_{i=0}^{\infty}\sum_{j=0}^{\infty}\sum_{k=0}^{\infty}\frac{(-1)^{i+j+k}}{i!\,j!\,k!}\ \xi_1^i\xi_2^j\xi_3^k\ \nabla_1^i\nabla_2^j\nabla_3^k\ \phi(\mathbf{x},t) \tag{4.3}$$

Considering the same filter moment definition as Eq. (3.4) TCE for unstructured grids are finally equal to:

$$\mathrm{TCE}[\phi] = \sum_{i=0}^{\infty}\sum_{j=0}^{\infty}\sum_{k=0}^{\infty}\frac{(-1)^{i+j+k}}{i!\,j!\,k!}\ \frac{\partial}{\partial t}\left[\mathcal{M}^{(ijk)}\right]\nabla_1^i\nabla_2^j\nabla_3^k\ \phi(\mathbf{x},t) \tag{4.4}$$

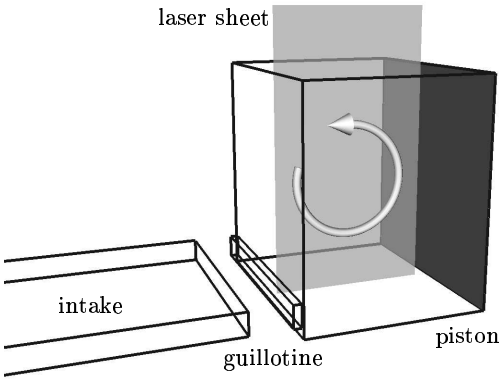

FIGURE 1. Square-piston experiment sketch.

It is important to note that in Eq. (4.4) the different TCE contributions from the cell deformation or from the filter shape variations can not be analysed separately like in the structured case. They are all included in the filter moment derivative $\partial \mathcal{M}^{(ijk)}/\partial t$.

5. Evaluation of TCE on a piston-engine like configuration

The choice of a piston-engine like configuration to evaluate the TCE magnitude has been guided by the following considerations :

- geometrical simplicity to avoid meshing issues,
- four-stroke operating mode to have a piston-engine like behaviour in terms of pressure and density variations,
- availability of experimental measurements to validate numerical simulations.

5.1. *Description of the square-piston experiment*

The square-piston experiment has been designed and operated at Institut de Mécanique des Fluides de Toulouse (IMFT) to study the compression and the disruption of tumble vortices that occur in Spark-Ignition (SI) engines (Marc *et al.* 1997; Boree *et al.* 2002). This device has been specifically designed to validate LES computations, offering many Particle Image Velocimetry (PIV) measurements for different piston positions. This experiment consists of :

- a square piston that has a sinusoidal motion,
- a rectangular intake channel that is also used as exhaust channel,
- a guillotine that closes the intake channel during compression and expansion strokes,
- a plenum at constant pressure connected to the intake channel.

A sketch of this experiment is given on Fig. (1). The position of the intake channel on the chamber head ensures the generation of a strong tumble motion that is then compressed when the guillotine is closed. Because of synchronisation issues between the PIV device and the piston position, the crank speed is very moderate at 206 rotations per minute (rpm). The compression ratio t_c is equal to 4 and the stroke is 75 mm long. The dimensions of the piston are $100\times100\,mm^2$ and those of the channel are $300\times96\times10\,mm^3$. PIV measurements are done in the symmetry plane of the configuration, where two velocity components are available. For each chosen piston position more than one hundred instantaneous PIV shots are available. Mean and fluctuating fields computed from these are also available.

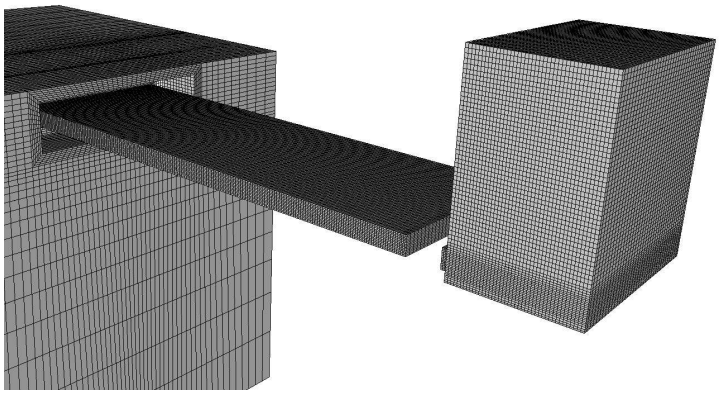

FIGURE 2. Square-piston experiment mesh comprising combustion chamber, intake channel and plenum.

5.2. *Large-Eddy Simulation computations*

5.2.1. *Code description*

The AVBP code (*http://www.cerfacs.fr/cfd/softwares.php*) is used for the following LES computations. This tool is co-developed by CERFACS and IFP and target applications are gas turbines, rocket propellers and piston engines. AVBP solves explicitly the full compressible Navier-Stokes equations on unstructured hybrid 2D and 3D meshes. To better predict the combustion process in industrial applications the heat capacities of the flow can vary in function of temperature and composition. Sensible energy and enthalpy of each species are therefore tabulated for a wide temperature range and mean quantities (molecular weight, mean heat capacities, mean heat capacity ratio) are calculated according to the species mixing. Both second-order and third-order convective schemes (Colin & Rudgyard 2000) are available. These schemes and the NSCBC-based boundary conditions (Poinsot & Lele 1992) have been improved (Moureau *et al.* 2004) to deal with variable heat capacities.

AVBP offers different turbulent models such as the Smagorinsky model (Smagorinsky 1963) or the WALE model (Nicoud & Ducros 1999). Flame/turbulence interactions are taken into account by the thickened flame model (Angelberger *et al.* 2000; Colin *et al.* 2000; Légier *et al.* 2000).

5.2.2. *Numerical set-up*

3D simulations have been carried out on relatively coarse grids, *i.e.* between 250000 and 300000 cells for the whole device (see Fig. (2)). Because of the combustion chamber compression the grid connectivity has to be modified during the computations to keep a reasonable mesh quality. At several times during the simulations cells are removed or added, the mesh is remapped and the flow is interpolated from the old to the new mesh. The number of connectivity changes is conditionned by the compression ratio as shown on Fig. (3). It represents a mean cell width $\delta = V_\omega^{1/3}$ as a function of the crank angle before top-dead center (BTDC) during the compression stroke. The discontinuities on both curves correspond to connectivity changes, which occur more often for $t_c = 10$.

5.2.3. *Validation of LES simulations*

LES simulations are validated performing the comparison with PIV data of the square-piston experiment. LES computations have been carried out with the Lax-Wendroff con-

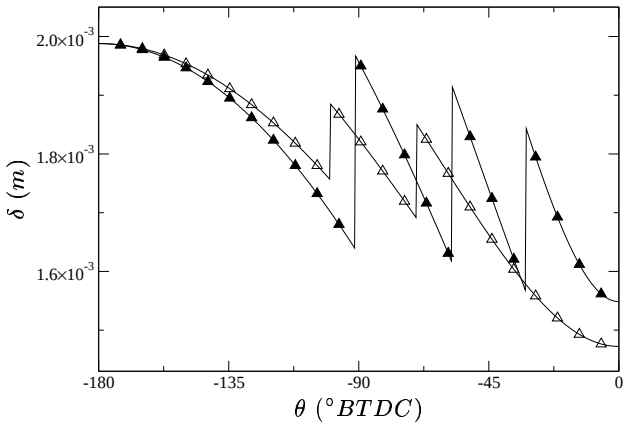

FIGURE 3. Evolution of the mean cell width δ during the compression stroke. —△—: $t_c = 4$; —▲—: $t_c = 10$.

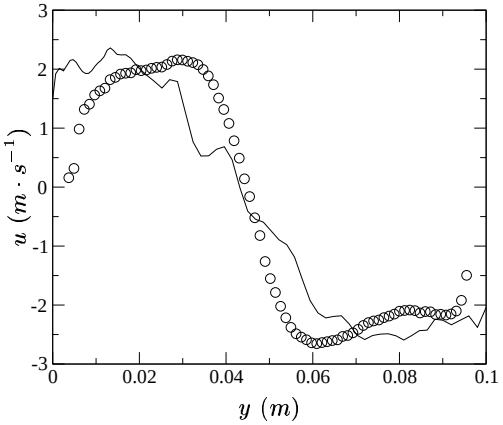

FIGURE 4. Middle x-plane mean profile. ∘ : experiments ; —— : LES.

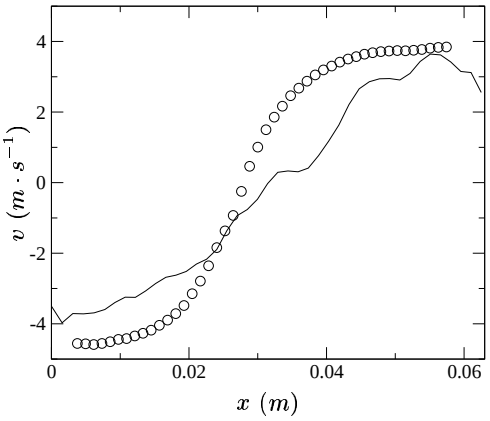

FIGURE 5. Middle y-plane mean profile. ∘ : experiments ; —— : LES.

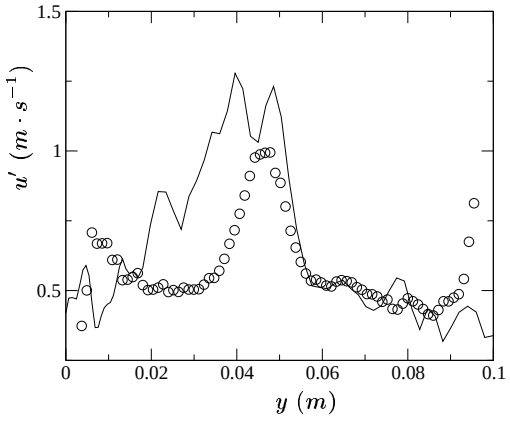

FIGURE 6. Middle x-plane fluctuation profile. ∘ : experiments ; —— : LES.

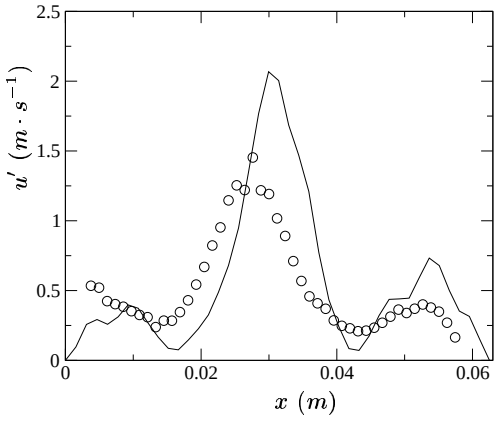

FIGURE 7. Middle y-plane fluctuation profile. ∘ : experiments ; —— : LES.

vective scheme, the Smagorinsky model and a simple logarithmic wall-law model. Six consecutive LES cycles are averaged to obtain mean and fluctuation profiles. Results at the half of the compression stroke ($-90°BTDC$) are presented on Fig. (4) to Fig. (7). Fig. (4) and Fig. (5) show the mean velocity profiles in the middle of the symmetry plane whereas Fig. (6) and Fig. (7) represent resolved velocity fluctuations u' in the same location. Mean profiles are in good agreement with experimental data indicating that the tumble intensity is well predicted. The fact that the maxima of fluctuations occur at the center of the rotating tumble indicates that they are mainly due to the precession motion of the tumble. This is reproduced by the LES findings.

5.3. *Estimation of TCE*

5.3.1. *Filter choice for the TCE evaluation*

As stated in Section 4 mesh cells do not have orthogonal main directions on unstructured grids and the filter can not be written as the combination of three filters in each main direction. Different filters for unstructured grids are found in the litterature. For instance filters that commute with spatial partial derivatives are based on weighting functions of surrounding nodes (Vasilyev *et al.* 1998; Vasilyev & Goldstein 2004). Filters have to satisfy several properties to be usable for LES :

- integral over the domain must be unity,
- filter shape has to be well defined and not to vary too much in space
- filter support has to be as compact as possible for practical calculation issues

The simplest filter for LES computations on unstructured grids is the Gaussian filter. This filter needs a characteristic length that can be expressed as a function of the cell volume $\Delta(\mathbf{x},t) = \delta(\mathbf{X},t) = V^{\frac{1}{3}}(\mathbf{X},t)$:

$$G(\boldsymbol{\xi},\mathbf{x},t) = \left(\frac{6}{\pi}\right)^{\frac{3}{2}} \frac{1}{\Delta^3(\mathbf{x},t)} \exp\left(-6\,\frac{\xi_1^2+\xi_2^2+\xi_3^2}{\Delta^2(\mathbf{x},t)}\right) \tag{5.1}$$

This filter satisfies $\mathcal{M}^{(0,0,0)} = 1$ and since this filter is symmetric the first non-zero moments are $\mathcal{M}^{(2,0,0)} = \mathcal{M}^{(0,2,0)} = \mathcal{M}^{(0,0,2)} = \Delta^2/12$.

5.3.2. *TCE modeling*

The only mean to evaluate exactly the TCE magnitude would be to perform a DNS of the square-piston engine experiment. Since this is not feasible a TCE model for the momentum equation is proposed and evaluated on LES simulations. TCE are indeed appearing on the whole Navier-Stokes equations but without combustion, spatial variations of density ρ and total energy ρE are small compared to momentum $\rho\mathbf{u}$ variations.

The simpliest TCE modeling is to keep only the leading terms of Eq. (4.4). This is reasonable since the main LES hypothesis requires that the filter width should be noticeably smaller than the integral length scale. In this case the higher-order terms in Eq. (4.4) are negligible compared to the leading terms. For the Gaussian filter defined on Eq. (5.1) the proposed model is thus :

$$\mathrm{TCE}[\phi] = \frac{1}{12}\Delta\frac{\partial\Delta}{\partial t}\boldsymbol{\nabla}\cdot(\boldsymbol{\nabla}\phi(\mathbf{x},t)) \tag{5.2}$$

Then if the filter width is a function of the local cell width it is more convenient to do the same decomposition as Eq. (2.10) :

$$\mathrm{TCE}[\phi] = \frac{\delta}{12}\Big(\dot{\mathbf{X}}\cdot\boldsymbol{\nabla}\delta\Big)\boldsymbol{\nabla}\cdot(\boldsymbol{\nabla}\phi(\mathbf{x},t)) + \frac{\delta^2}{12}\Big(\frac{1}{3}\overline{\boldsymbol{\nabla}\cdot\dot{\mathbf{X}}}\Big)\boldsymbol{\nabla}\cdot(\boldsymbol{\nabla}\phi(\mathbf{x},t)) \tag{5.3}$$

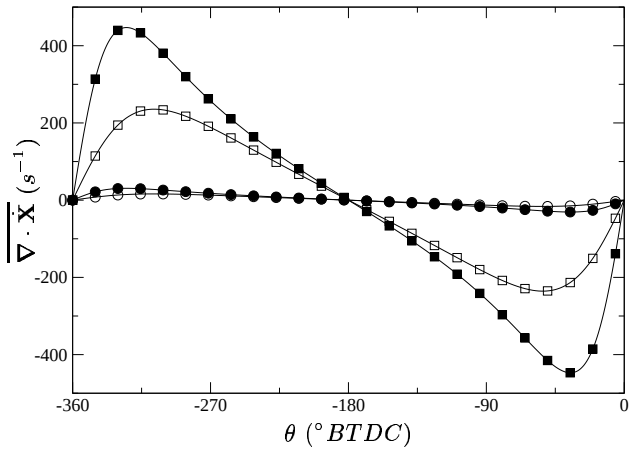

FIGURE 8. $\overline{\nabla \cdot \dot{\mathbf{X}}}$ as a function of crank angle. —○—: 206 *rpm* , $t_c = 4$; —●—: 206 *rpm* , $t_c = 10$; —□—: 3000 *rpm* , $t_c = 4$; —■—: 3000 *rpm* , $t_c = 10$.

The first term of Eq. (5.3) is a spatial commutation error that vanishes when the cell width δ is uniform. Only the second right-hand term is of interest in this study. This term is a diffusion or anti-diffusion term depending on the sign of the factor $\delta^2(\overline{\nabla \cdot \dot{\mathbf{X}}})/36$ that has the dimension of a viscosity. In this factor δ^2 is almost constant during the simulation thanks to connectivity changes as shown on Fig. (3). The mean deformation rate $\overline{\nabla \cdot \dot{\mathbf{X}}}$ depends only on engine parameters such as crank speed and compression ratio t_c. This dependence is illustrated on Fig. (8) for a simple sinusoidal law during intake ($\theta \in [-360°, -180°]$) and compression ($\theta \in [-180°, 0°]$) strokes. This rate expressed as a function of the crank angle scales linearly with crank speed and non-linearly with compression ratio.

5.3.3. *Evaluation in the code*

TCE are evaluated in the LES code only for the momentum equation. As seen in Section 5.3.2 TCE on unstructured grids with a Gaussian filter are diffusive or anti-diffusive. It means that the effective momentum diffusion in a LES simulation will be the sum of the molecular, turbulent and TCE diffusion. Since momentum diffusion corresponds to kinetic energy dissipation a good mean to compare the turbulent diffusion to the TCE diffusion is to study the ratio $\mathcal{R}$ between the resolved kinetic energy dissipated by TCE and by molecular plus turbulent diffusion :

$$\mathcal{R} = \frac{\left\langle \bar{u}_i \, \frac{\delta^2}{12} \left(\frac{1}{3} \overline{\nabla \cdot \dot{\mathbf{X}}} \right) \nabla \cdot (\nabla \bar{\rho} \bar{u}_i) \right\rangle}{\left\langle \bar{u}_i \frac{\partial \bar{\tau}_{ij}}{\partial x_j} + \bar{u}_i \frac{\partial \bar{t}_{ij}}{\partial x_j} \right\rangle} \tag{5.4}$$

where the brackets <> correspond to the spatial averaging operator. In Eq. (5.4) the different terms are not proper dissipation rates but the sum of kinetic energy dissipation rates plus kinetic energy transport by momentum diffusion :

$$\left\langle \bar{u}_i \frac{\partial \bar{\tau}_{ij}}{\partial x_j} \right\rangle = \left\langle -\frac{\partial \bar{u}_i}{\partial x_j} \bar{\tau}_{ij} \right\rangle + \left\langle \frac{\partial \bar{u}_i \bar{\tau}_{ij}}{\partial x_j} \right\rangle \tag{5.5}$$

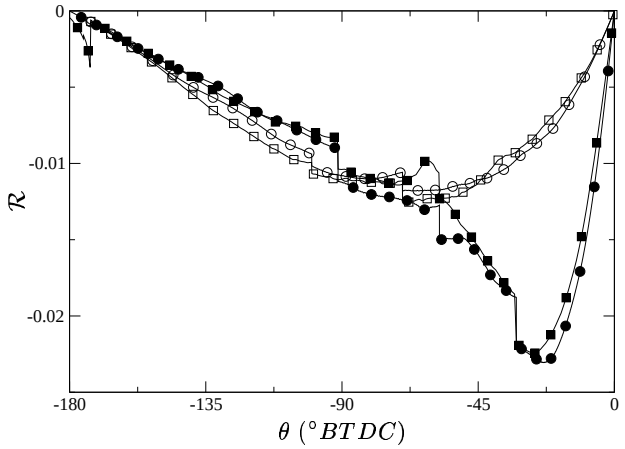

FIGURE 9. Ratio $\mathcal{R}$ of TCE and molecular plus turbulent dissipations as a function of crank angle. —○—: 206 *rpm* , $t_c = 4$; —●—: 206 *rpm* , $t_c = 10$; —□—: 3000 *rpm* , $t_c = 4$; —■—: 3000 *rpm* , $t_c = 10$.

The second right-hand term of Eq. (5.5) is a boundary term that is nearly zero and $\mathcal{R}$ is therefore a dissipation ratio.

Four single-cycle simulations have been performed to evaluate TCE and the effect of the crank speed and of the compression ratio. Results are presented on Fig. (9). The first remark is that the TCE levels are small compared to molecular plus turbulent dissipation. A maximum of about 1.2% for $t_c = 4$ and 2.5% for $t_c = 10$ is found at the end of the compression stroke. The second remark is that the evaluated ratio $\mathcal{R}$ does only marginally depend on crank speed. It means that TCE and physical dissipation scale in the same manner relatively to crank speed. This is not the case for the compression ratio, leading to some differences at the end of the compression stroke when almost all resolved eddies have been dissipated. Compared to the numerical dissipation of numerical schemes and other uncertainties, TCE can therefore be neglected for applications that operate in about the same range of parameters.

6. Conclusions

TCE have been derived for structured and unstructured grids and models have been proposed. These models have been evaluated on a square-piston experiment and it was shown that kinetic energy dissipation due to TCE can be neglected compared to the turbulent dissipation in piston-engine like applications. It should be underlined that in piston-engines the flow and the mesh deformation are generated by the same phenomenon that is the piston motion. But in some other cases as flame computations with automatic local mesh refinement, TCE are not correlated anymore to local turbulence and they may not remain negligible.

REFERENCES

ANGELBERGER, C., VEYNANTE, D. & EGOLFOPOULOS, F. 2000 LES of chemical and acoustic forcing of a premixed dump combustor. *Flow Turb. Comb.* **65** (2), 205–222.

BOREE, J., MAUREL, S. & BAZILE, R. 2002 Disruption of a compressed vortex. *Phys. Fluids* **14** (7), 2543–2556.

Celik, I., Yavuz, I. & Smirnov, A. 2001 Large Eddy Simulations of In-Cylinder turbulence for IC engines: A review. *Int. J. of Engine Research* **2** (2).

Colin, O., Ducros, F., Veynante, D. & Poinsot, T. 2000 A thickened flame model for LES of turbulent premixed combustion. *Phys. Fluids* **12** (7), 1843–1863.

Colin, O. & Rudgyard, M. 2000 Development of high-order Taylor-Galerkin schemes for LES. *J. Comp. Phys.* **162** (2), 338–371.

Franke, J. & Frank, W. 2001 Temporal commutation errors in Large-Eddy Simulation. *Zeitschrift Fur Angewandte Mathematik Und Mechanik* **81** (S3), S467–S468.

Fureby, C. & Tabor, D. 1997 Mathematical and physical constraints on Large-Eddy Simulations. *Theor. Comp. Fluid Dyn.* **9** (2), 85–102.

Ghosal, S. 1999 Mathematical and physical constraints on Large-Eddy Simulation of turbulence. *AIAA J.* **37** (4), 425–433.

Ghosal, S. & Moin, P. 1995 The basic equations for the Large-Eddy Simulation of turbulent flows in complex-geometry. *J. Comp. Phys.* **118** (1), 24–37.

Haselbacher, A. & Vasilyev, O. 2003 Commutative discrete filtering on unstructured grids based on least-squares techniques. *J. Comp. Phys.* **187** (1), 197–211.

Kaufmann, A., Nicoud, F. & Poinsot, T. 2002 Flow forcing techniques for numerical simulation of combustion instabilities. *Comb. Flame* **131**, 371–385.

Légier, J.-P., Poinsot, T. & Veynante, D. 2000 Dynamically thickened flame LES model for premixed and non-premixed turbulent combustion. In *Proc. 2000 Summer Program*, pp. 157–168. Center for Turbulence Research, Stanford, USA.

Marc, D., Boree, J., Bazile, R. & Charnay, G. 1997 PIV and LDV measurements of tumbling vortex flow in a model square section motored engine. *Soc. Auto. Eng.* Paper (972834).

Marsden, A., Vasilyev, O. & Moin, P. 2002 Construction of commutative filters for LES on unstructured meshes. *J. Comp. Phys.* **175** (2), 584–603.

Moureau, V., Lartigue, G., Sommerer, Y., Angelberger, C., Colin, O. & Poinsot, T. 2004 Numerical methods for unsteady compressible multi–component reacting flows on fixed and moving grids. *accepted for publication in J. Comp. Phys.* .

Nicoud, F. & Ducros, F. 1999 Subgrid-scale stress modelling based on the square of the velocity gradient tensor. *Flow Turb. Comb.* **62** (3), 183–200.

Poinsot, T. & Lele, S. 1992 Boundary conditions for direct simulations of compressible viscous flows. *J. Comp. Phys.* **101** (1), 104–129.

Prière, C., Gicquel, L. Y. M., Kaufmann, A., Krebs, W. & Poinsot, T. 2004 LES of mixing enhancement : LES predictions of mixing enhancement for jets in cross-flows. *J. Turb.* **5**, 1–30.

Selle, L., Lartigue, G., Poinsot, T., Koch, R., Schildmacher, K.-U., Krebs, W., Prade, B., Kaufmann, P. & Veynante, D. 2004 Compressible Large-Eddy Simulation of turbulent combustion in complex geometry on unstructured meshes. *Comb. Flame* **137** (4), 489–505.

Smagorinsky, J. 1963 General circulation experiments with the primitive equations: 1. the basic experiment. *Mon. Weath. Rev.* **91**, 99–164.

Vasilyev, O. & Goldstein, D. 2004 Local spectrum of commutation error in Large Eddy Simulations. *Phys. Fluids* **16** (2), 470–473.

Vasilyev, O., Lund, T. & Moin, P. 1998 A general class of commutative filters for LES in complex geometries. *J. Comp. Phys.* **146** (1), 82–104.